Annales Geophysicae (2002) 20: 427–444 © European Geophysical Society 2002

Annales Geophysicae

Particle transport in ^{3}He-rich events: wave-particle interactions and particle anisotropy measurements

B. T. Tsurutani[1], L. D. Zhang[1], G. L. Mason[2,3], G. S. Lakhina[4], T. Hada[5], J. K. Arballo[1], and R. D. Zwickl[6]

[1]Jet Propulsion Laboratory, California Institute of Technology, Pasadena, California, USA
[2]Department of Physics, University of Maryland, College Park, Maryland, USA
[3]Institute for Physical Science and Technology, University of Maryland, College Park, Maryland, USA
[4]Indian Institute of Geomagnetism, Colaba, Mumbai/Bombay, India
[5]Earth System Science Technology, Kyushu University, Kasuga, Japan
[6]National Oceanic and Atmospheric Administration, Space Environment Laboratory, Boulder, Colorado, USA

Received: 29 May 2000 – Revised: 7 November 2001 – Accepted: 8 November 2001

Abstract. Energetic particles and MHD waves are studied using simultaneous ISEE-3 data to investigate particle propagation and scattering between the source near the Sun and 1 AU. ^{3}He-rich events are of particular interest because they are typically low intensity "scatter-free" events. The largest solar proton events are of interest because they have been postulated to generate their own waves through beam instabilities. For ^{3}He-rich events, simultaneous interplanetary magnetic spectra are measured. The intensity of the interplanetary "fossil" turbulence through which the particles have traversed is found to be at the "quiet" to "intermediate" level of IMF activity. Pitch angle scattering rates and the corresponding particle mean free paths λ_{W-P} are calculated using the measured wave intensities, polarizations, and $\boldsymbol{k}$ directions. The values of λ_{W-P} are found to be ~ 5 times less than the value of λ_{He}, the latter derived from He intensity and anisotropy time profiles. It is demonstrated by computer simulation that scattering rates through a 90° pitch angle are lower than that of other pitch angles, and that this is a possible explanation for the discrepancy between the λ_{W-P} and λ_{He} values. At this time the scattering mechanism(s) is unknown. We suggest a means where a direct comparison between the two λ values could be made. Computer simulations indicate that although scattering through 90° is lower, it still occurs. Possibilities are either large pitch angle scattering through resonant interactions, or particle mirroring off of field compression regions.

The largest solar proton events are analyzed to investigate the possibilities of local wave generation at 1 AU. In accordance with the results of a previous calculation (Gary et al., 1985) of beam stability, proton beams at 1 AU are found to be marginally stable. No evidence for substantial wave amplitude was found. Locally generated waves, if present, were less than 10^{-3} nT^2 Hz^{-1} at the leading proton event edge, where dispersion effects (beaming) are the greatest, and at the point of peak proton flux, where the particle energy flux is the greatest.

Key words. Interplanetary physics (energetic particles; MHD waves and turbulence) – Space plasma physics (charged particle motion and acceleration; wave-particle interactions)

Correspondence to: B. T. Tsurutani
(bruce.tsurutani@jpl.nasa.gov)

1 Introduction

The transport of solar cosmic rays in the heliosphere is a fundamental problem, not only for understanding the evolution of propagation of such particles from the Sun to 1 AU, but also for understanding properties of the interplanetary medium through which the energetic particles have passed. Because the solar particle energy densities are low compared to the ambient interplanetary magnetic field densities, the particles are guided by the field lines, which typically have the shape of a Parker spiral (Thomas and Smith, 1980). Low frequency (LF) electromagnetic waves which are present on these field lines can cyclotron resonate with the solar particles, scattering them in a pitch angle. If the resonant waves are particularly intense, both diffusion in pitch angle and diffusion across magnetic field lines can occur (Tsurutani and Lakhina, 1997). The LF waves can be of the "fossil" type, where fluctuations originating in the lower corona are convected outward by the solar wind (Coleman, 1968; Belcher and Davis, 1971; Tsurutani et al., 1994; Smith et al., 1995; Balogh et al., 1995; Tsurutani et al., 2001) with subsequent nonlinear evolution to a turbulent spectrum (Roberts and Goldstein, 1991; Bavassano and Bruno, 1991; Tu and Marsch, 1993). In either case (fossil waves or turbulence), this type of wave-particle interaction is called "parasitic".

Table 1. ^{3}He-rich scatter-free events

Event	Date	Event onset		Event end		Velocity dispersion	Mean free path λ (AU)	Comments
		Day	Time	Day	Time			
1	23 Oct 1978	296	1400		2200	yes	> 1.0	
2	26 Dec 1978	360	1600	361	1500	yes	1.0	
3	17 May 1979	137	0630		2200	yes	0.5	
4	14 Dec 1979	348	2000	349	1100	yes	2.0	
5	13 Jan 1980	013	2200	014	0800	yes	> 0.5	other activity
6	9 Nov 1980	314	1100		2200	no	> 0.3	shock
7	31 Jul 1981	212	0200	213	1630	?	> 0.5	data gaps
8	12 Feb 1982	043	2000	044	1700	?	> 0.5	other activity

Some part of the wave power could also be generated by solar flare particles themselves, through a beam instability (Reames, 1989; Ng and Reames, 1994) if the beam intensity is sufficiently high or sufficiently anisotropic (see also Gary et al., 1985). However, Valdes-Galicia and Alexander (1997) and Alexander and Valdes-Galicia (1998) have made a search for self-generated waves near the maximum observed flux of the proton events in the Helios (0.3 to 1.0 AU) data set. Their Elasser variable analyses indicated a lack of sufficient self-generated wave power "to make a contribution to solar cosmic ray transport".

In the past, particle transport from the solar corona to 1 AU has been studied by inferring the amount of pitch angle scattering that has taken place from an analysis of the particle distributions themselves, or by taking a characteristic interplanetary wave spectrum and theoretically calculating the amount of scattering that should have taken place assuming that the spectrum is representative (for example, see Jokipii and Coleman, 1968; Zwickl and Webber, 1977; Ma Sung and Earl, 1978; Beeck et al., 1987; Mason et al., 1989; Beeck et al., 1990; Tan and Mason, 1993). For a detailed discussion of the two methods, see Palmer (1982) and Wanner and Wibberenz (1993). Calculation of the energetic particle scattering mean free paths using the magnetic field data and a quasi-linear theory of the field fluctuations has led to a long-standing discrepancy wherein this calculated mean free path is generally much smaller than the mean free paths calculated using particle measurements (Palmer, 1982). Some recent theoretical studies (Schlickeiser, 1989; Schlickeiser and Miller, 1998) have obtained improved results (i.e. larger calculated particle scattering mean free paths) by using more complex models for the waves. Wanner et al. (1994) presented evidence showing that the "slab" turbulence approximation was fundamentally flawed, and this was followed by Bieber et al. (1996), who showed that two-dimensional (2D) turbulence was playing a major role. Bieber et al. (1996) applied a 2D model to ~ 10 MeV proton observations from Helios and found good agreement between the mean free paths calculated from the turbulence and from the energetic particle observations.

It is known that the amount of wave power present in the interplanetary medium is highly variable, varying by orders of magnitude depending on the type of solar wind (Siscoe et al., 1968; Belcher and Davis, 1971; Smith et al., 1995). The Ulysses mission has particularly emphasized this point by indicating the continuous, high intensity Alfvén waves present in high-speed streams coming from coronal holes (Balogh et al., 1995; Phillips et al., 1995).

It is the purpose of this paper to examine the simultaneous 1 AU LF wave properties (at frequencies near the particle cyclotron resonance) during two specific types of solar particle events: 1) ^{3}He-rich events which propagate from the Sun to 1 AU and have large front-to-back particle anisotropies, and 2) the largest intensity ISEE-3 solar proton events where there is the possibility of in-situ wave generation by proton-proton beam instabilities themselves. The former (^{3}He-rich) events are of particular interest because they appear to propagate "without scatter". The latter events are interesting because they may be a source for waves in the interplanetary medium, and also if generation does occur, they would be a potential source of waves for parasitically scattering the He ions. For both parts of this study, we use well-established, previously identified solar energetic particle events. The solar energetic particles used in this study have energies near 1 MeV/nucleon, considerably lower than the ~ 1020 MeV energies of the recent comprehensive propagation studies (Wanner and Wibberenz, 1993; Bieber et al., 1996), and therefore their resonant scattering studies probe a higher frequency portion of the IMF wave spectrum.

2 Method of analyses

To examine simultaneous wave and solar energetic particle events, we use the ISEE-3 1 AU data from the magnetometer instrument (Frandsen et al., 1978) and the Ultra Low Energy Wide Angle Telescope (ULEWAT) instrument (Hovestadt et al., 1978). For the ^{3}He-rich events, we examine 8 of the examples previously published in Kahler et al. (1985). We have selected the events from the full Kahler et al. (1985) list on the basis of being able to obtain good signal-to-noise measurements from the ULEWAT instrument. The high intensity solar proton events were taken from the previously published

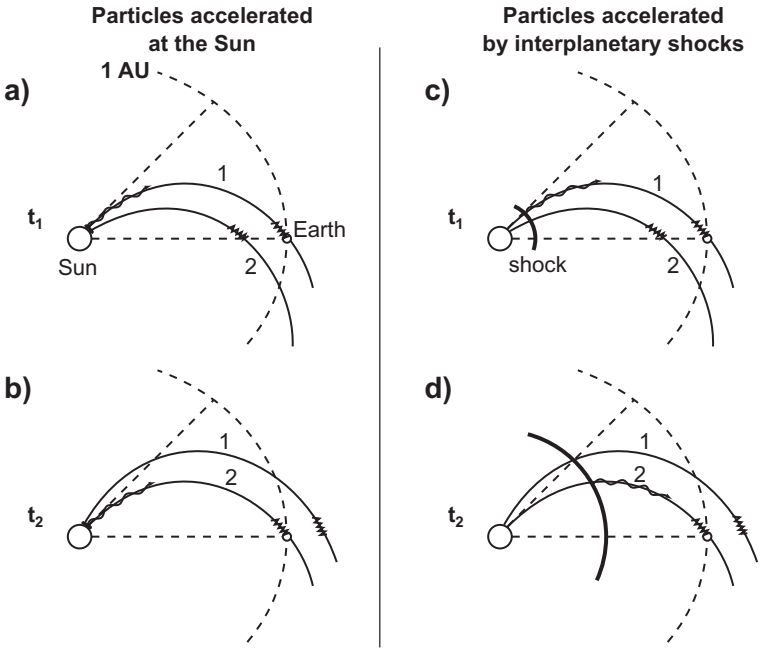

Fig. 1. The combined motion of radial expansion and corotation with the Sun causes the interplanetary field lines to continuously sweep past the Earth. Two magnetic field lines with Parker spiral configuration are illustrated in the panels of the figure. The dashed portion of the second field line is the part that is sampled at Earth in 1 day. Energetic particles (cyclical motion symbols) follow the magnetic field lines which corotate with the Sun. The fossil plasma waves (sawtooth symbols), however, are convected radially outward.

list of McGuire et al. (1986) (see also Mazur et al., 1992). We selected 7 of the most intense proton events from this ISEE-3 data set. Because the ion beam instability growth rates depend on the beam velocities, anisotropies, and energy densities, the largest solar particle events are the most likely to generate LF waves at 1 AU. We have chosen these most intense events to examine these possibilities.

A variety of magnetic field time scales was used. To compare the gross features of the particles and the magnetic fields, we use hourly averages. The field is plotted in ISEE-3 spacecraft coordinates, which are within 1° of the GSE coordinate system. In this system, $\boldsymbol{x}$ is the direction from the Earth towards the Sun, $\boldsymbol{y}$ is in the direction of $\Omega \times \boldsymbol{x}$, where the Ω vector is the north ecliptic pole, and $\boldsymbol{z}$ forms a right-hand system. To search for waves, we have used both the highest time resolution available, 6 vectors s^{-1}, and also one minute averages. Field-aligned one minute averaged transverse power spectra are used for the ^{3}He-rich events analyses, and the highest resolution data was used for the search of self-generated waves during the proton events. The latter data (high rate) was used to be able to identify specific wave polarizations (use of minimum variance analyses), wave $\boldsymbol{k}$, and frequency to positively identify the wave mode and generation mechanism.

Four energetic particle channels are used: 0.4–0.6 MeV/nucleon He, 0.6–1.0 MeV/nucleon He, 1.0–1.8 MeV/nucleon He, and a 10–20 MeV/nucleon proton channel (these He particle channels cover the sum of ^{3}He and ^{4}He particles; since the ^{3}He/^{4}He ratio averages ~ 2 in the events of Table 1, ^{3}He typically accounts for $\sim 2/3$ of the detections). Model fits to the energetic particle data are constructed to estimate the mean free paths associated with wave-particle interactions. The particle transport is described in terms of a Boltzmann equation which includes adiabatic focusing. A Parker spiral field configuration is assumed, as well as a constant rate of pitch angle scattering as a function of r, the distance from the Sun. Particle event onset times were taken from experimentally determined values of the Type III radio bursts. For more details of the assumptions/caveats made in the model, we refer the reader to Mason et al. (1989). These values will be compared with independent determinations made from the measured transverse wave power spectral densities. From theoretical expressions of the pitch angle scattering rates (Kennel and Petschek, 1966; Tsurutani and Lakhina, 1997), pitch angle diffusion will be calculated based on the measured wave power at the resonant frequencies. We consider only first-order cyclotron resonance because higher order resonances are much weaker.

3 Geometry

Figure 1 gives the geometry of the interplanetary magnetic field lines (assuming a Parker spiral), the rotation of the Earth about the Sun, and some pertinent velocities and time scales. The energetic ^{3}He ions propagate from the Sun to 1 AU in a relatively short amount of time, on the order of $\sim$10 hours. Specifically, a ~ 1 MeV/nucleon ^{3}He ion takes ~ 6 hours to propagate to 1 AU, assuming that it propagates along a spiral magnetic field line. Alfvén waves propagate at ~ 70 km s^{-1} at 1 AU, and the solar wind plasma propagates at a velocity of about 400 km s^{-1}. Thus to first order, the waves can be thought to be simply convected outward by the solar wind. It takes the solar wind propagation time ~ 4.3 days to reach the Earth (assuming $V_{SW} \approx 400$ km s^{-1}), much longer than the energetic particle transit time.

The interplanetary magnetic field typically has a Parker spiral geometry and thus does not allow one to measure all of the waves through which the particles have passed. This can be visualized in panel (a) by examining the single magnetic field line (solid spiral in Fig. 1) that extends from the Sun and passes through the Earth (labelled "1"). This schematic assumes that the particles are generated near the Sun. The particles that are detected by the spacecraft particle instrument are schematically denoted by their "cyclotron motions". The fossil waves convected by the solar wind to the spacecraft are denoted by a "sawtooth symbol". Although the LF waves that the particles pass through at 1 AU can be measured by ISEE-3, waves closer to the Sun occur at different solar longitudes (solid spiral 2). On the other hand, the duration of large solar particle events is from 12 hours to many days. Thus, if one examines the interplanetary magnetic fields throughout the entire particle event, one can examine the LF waves through which particles of the event have passed. From the schematic in Fig. 1 shown at a later time t_2, it can be noted that this is about the outermost ~ 0.25 AU of particle transport. Clearly, the entire ion path cannot be studied by this technique, but the outermost $\sim$0.25 AU gives some general idea of wave conditions through which the particles have propagated. Panels (c) and (d) depict particles being accelerated by an outward propagating interplanetary shock. Other features of these panels are the same as for panels (a) and (b).

4 Results

4.1 ^{3}He-rich events

Table 1 lists eight ^{3}He-rich events occurring between 1978 and 1982. The approximate particle event onset and termination times are listed for reference. The 7th column denotes whether velocity dispersion at the leading edge of the event is apparent or not. This will be an important indicator of the source of the particles as we will see later. Column 8 lists deduced particle mean free paths (λ_{He}) for the He events.

Figure 2 shows the 17 May 1979 energetic ion event. The three He energy channels are given in the top panel. Velocity dispersion is clearly present, with the highest energy particles arriving first, as expected for propagation from a remote source. The magnetic field is given in the middle four panels. The field is relatively quiet during the particle onset. The fluctuations in the three components are small, and the field magnitude is relatively low, ~ 4 to 5 nT. An examination of the solar wind velocity indicates that this particle event occurred in the far trailing portion of a high velocity stream. This region is noted for a lack of large amplitude Alfvén waves and relatively quiet magnetic fields (Tsurutani et al., 1995).

To quantify the characteristics of the interplanetary fluctuations during this particle event, we have made power spectra of the magnetic field components and the magnitude. This is shown in Fig. 3. Here we have used a field-aligned coordi-

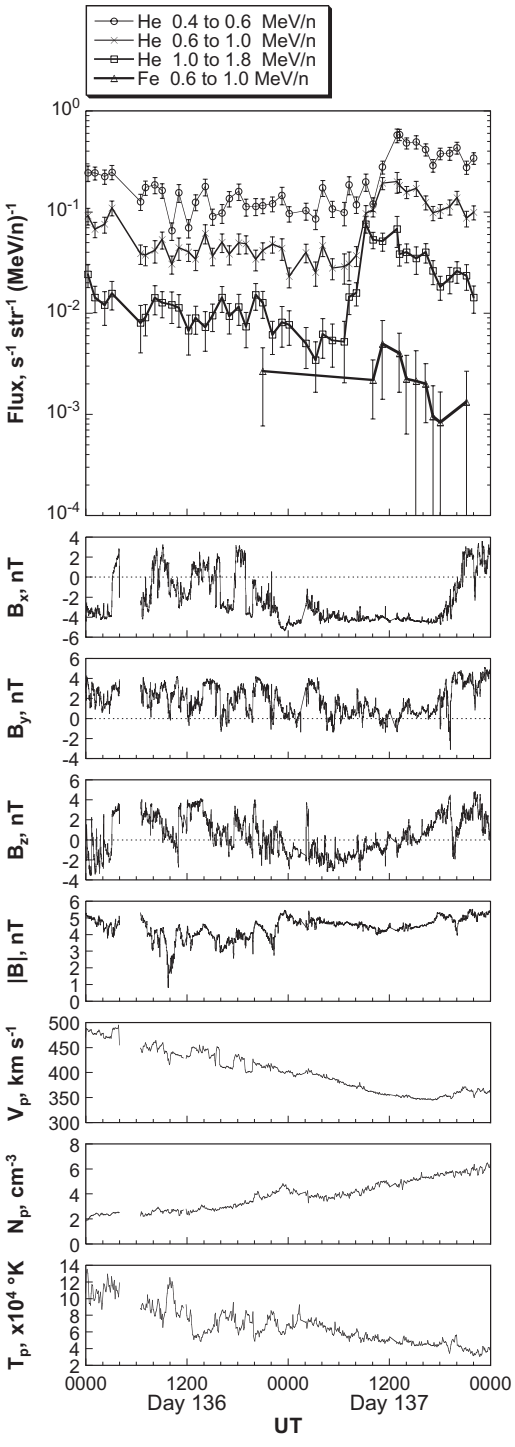

Fig. 2. Fluxes of energetic He (^{3}He+^{4}He) ions, and plasma and magnetic field parameters, plotted for the 17 May 1979 energetic ion event.

nate system, where B_1 is the field along the average magnetic field, B_2 is along the $(\boldsymbol{\Omega} \times \boldsymbol{B}_1)/|\boldsymbol{\Omega} \times \boldsymbol{B}_1|$ direction, where $\boldsymbol{\Omega}$ is the direction of the north solar pole, and B_3 completes the right-hand system. The power in the field magnitude is also given. The purpose of plotting the power spectra in these coordinates is to determine the power due to transverse fluctua-

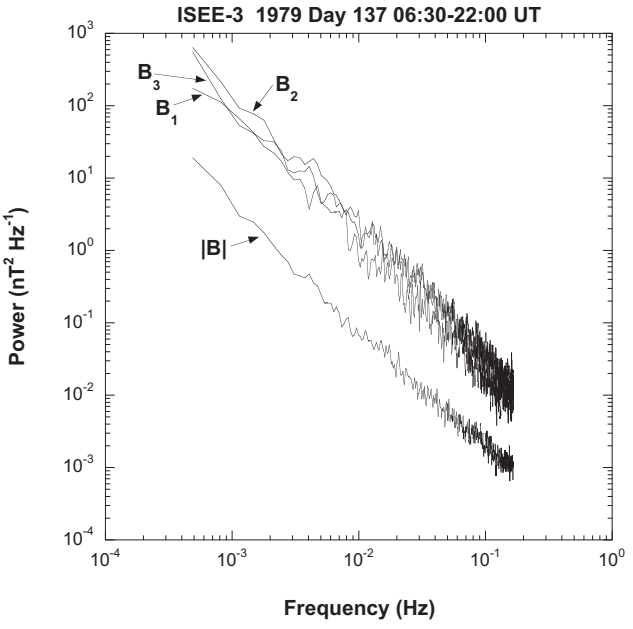

Fig. 3. Magnetic power spectra for the 17 May 1979 event. Components 1 and 2 are the two transverse components of the field.

tions (along B_2 and B_3) and the power due to compressional variations (in $|\boldsymbol{B}|$). The spectra of B_1, from a comparison to the spectra of $|B|$, can be used to determine how well the average field direction is maintained during the chosen interval. If the B_1 and $|B|$ power spectra are nearly identical, then the average field direction is a well-defined value. If, on the other hand, the B_1 power spectra were much larger than that of $|B|$ and were similar to the B_2 and B_3 spectra, this would indicate that the magnetic field direction is variable throughout the interval analyzed. This is the case here. These field directional changes can be noted in the middle panels of Fig. 2.

Comparing the four spectra, we find that most of the wave power is present in the transverse components. This power is ∼30 times the value of the compressional component. The power spectra exhibits no peaks of any significance. The transverse power can be characterized by $P^2 = 6.6 \times 10^{-4} f^{-1.8}\,\mathrm{nT}^2\ \mathrm{Hz}^{-1}$. The average magnetic field strength is $|B| = 4.6\,\mathrm{nT}$ (thus the normalized power spectra is $P^2 = 3.1 \times 10^{-5} f^{-1.8}\ \mathrm{Hz}^{-1}$). In comparison, Siscoe et al. (1968) reported a transverse power spectra of $P^2 = 8.2 \times 10^{-3} f^{-1.55}\,\mathrm{nT}^2\ \mathrm{Hz}^{-1}$ for "intense" events, $P^2 = 4.5 \times 10^{-3} f^{-1.51}\,\mathrm{nT}^2\ \mathrm{Hz}^{-1}$ for "moderate" events and $P^2 = 8.5 \times 10^{-4} f^{-1.59}\,\mathrm{nT}^2\ \mathrm{Hz}^{-1}$ for "quiet" intervals. The power spectra in Fig. 3 is thus consistent with quiet IMF activity. It is both lower in intensity and steeper in slope than the intense and moderate activity reported by Siscoe et al. (1968). The transverse power spectra will later be used for the calculations for first-order cyclotron resonant wave-particle interactions. These waves have previously been shown to be Alfvén waves with arc-polarization (Tsurutani et al., 1994). The compressional component of the

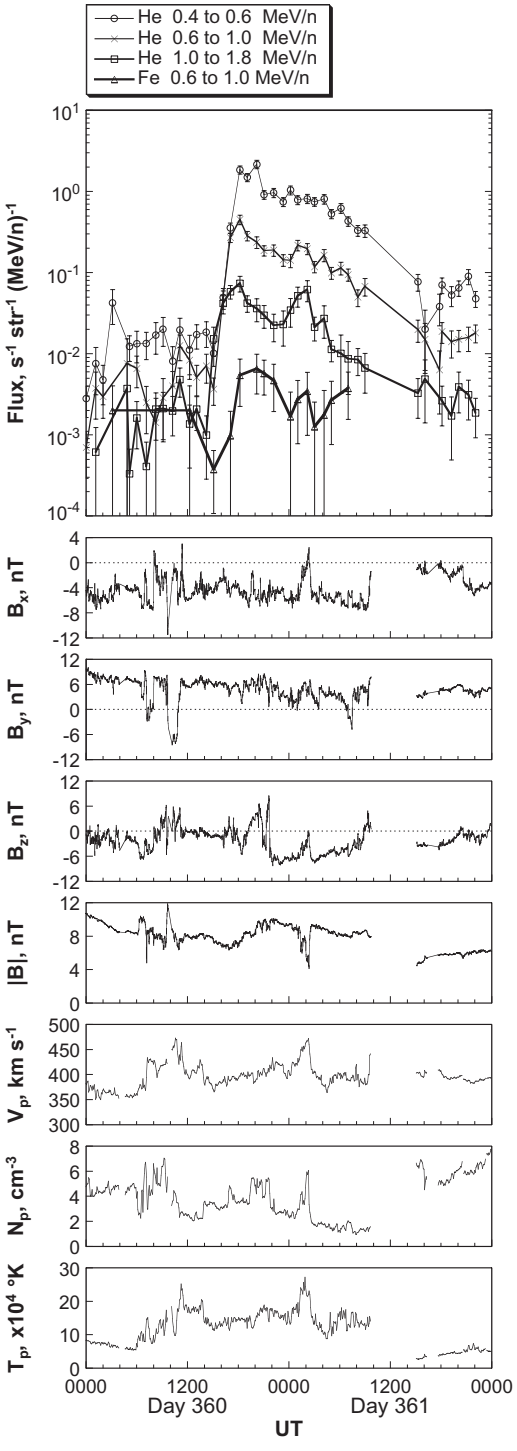

Fig. 4. He (^{3}He+^{4}He) flux, plasma and magnetic field data for the 26 December 1978 event.

field can be due to either the magnetosonic mode or convected static structures (see Tsurutani et al., 2001). It should be noted that clear magnetosonic mode waves have not been detected in the solar wind.

A second event, on 26 December 1978, is shown in Fig. 4. Again, there is clear velocity dispersion present in the energetic He ions. The magnetic field fluctuations are modest.

Table 2. Transverse power spectra for 8 scatter-free events

Event	Average transverse power (nT^2/Hz)	Average $\|\boldsymbol{B}\|$ (nT)	Normalized transverse power (Hz^{-1})
1	$3.26 \times 10^{-3} f^{-1.7}$	6.30	$8.21 \times 10^{-5} f^{-1.7}$
2	$2.81 \times 10^{-3} f^{-1.7}$	8.11	$4.27 \times 10^{-5} f^{-1.7}$
3	$6.58 \times 10^{-4} f^{-1.8}$	4.63	$3.06 \times 10^{-5} f^{-1.8}$
4	$7.43 \times 10^{-3} f^{-1.7}$	9.93	$7.54 \times 10^{-5} f^{-1.7}$
5	$1.89 \times 10^{-3} f^{-1.7}$	6.25	$4.84 \times 10^{-5} f^{-1.7}$
6	$4.82 \times 10^{-3} f^{-1.7}$	11.47	$3.66 \times 10^{-5} f^{-1.7}$
7	$3.60 \times 10^{-3} f^{-1.6}$	9.66	$3.86 \times 10^{-5} f^{-1.6}$
8	$1.08 \times 10^{-2} f^{-1.7}$	15.56	$4.46 \times 10^{-5} f^{-1.7}$

The wave power is determined to be $2.8 \times 10^{-3} f^{-1.7}$ nT^2 Hz^{-1} for the transverse components. In comparison to the Siscoe et al. (1968) values, the fluctuation spectra for this event is between moderate and quiet. The reader should note that the important quantity for particle scattering in quasi-linear theory is the normalized wave power. This is the power spectra divided by $|B|^2$. For resonant wave-particle interactions in quasi-linear theory, the pitch angle diffusion rate is proportional to $(\Delta B/|B|)^2$. For a detailed discussion, we refer the reader to Kennel and Petschek (1966) for pitch angle scattering, and Tsurutani and Thorne (1982), Tsurutani and Lakhina (1997), and Tsurutani et al. (2000) for cross-field diffusion. The average magnetic field magnitude during this event is $|B| = 8.1$ nT so the normalized power is $P^2 = 4.3 \times 10^{-5} f^{-1.7}$ Hz^{-1}. This is approximately of the same order of magnitude as that of the Fig. 3 event. There are some small velocity fluctuations from 07:00–14:00 UT, day 360 and ∼ 02:00 UT, day 361 but no major streams are present.

An examination of the power spectra of the field for all of the particle events has been performed. The results are shown in Table 2. In each case, it is found that the power is consistent with quiet to intermediate interplanetary conditions for all events except event 4 (day 348, 1979) and event 8 (day 212, 1981) where the power is more typical of an active interval. These two events will be discussed later.

One He event did not exhibit clear velocity dispersion: 9 November 1980. A second event (31 July 1981) could not be tested for velocity dispersion, due to data gaps.

The 9 November 1980 event (no. 6) is shown in Fig. 5. It can be clearly seen that the particle event onset occurs just after a sharp jump in field magnitude. This jump is denoted by a vertical dashed line. There are also simultaneous jumps in solar wind velocity, density, and temperature, indicating that this is a fast forward shock propagating in the antisunward direction. The energetic particle fluxes from 18:00 to 21:00 UT are nearly isotropic, in contrast to the large anisotropies observed in the other He events.

It should be noted that the particle event onset occurs almost at the same time as the shock. Several possible explanations exist. This event could be explained by the existence

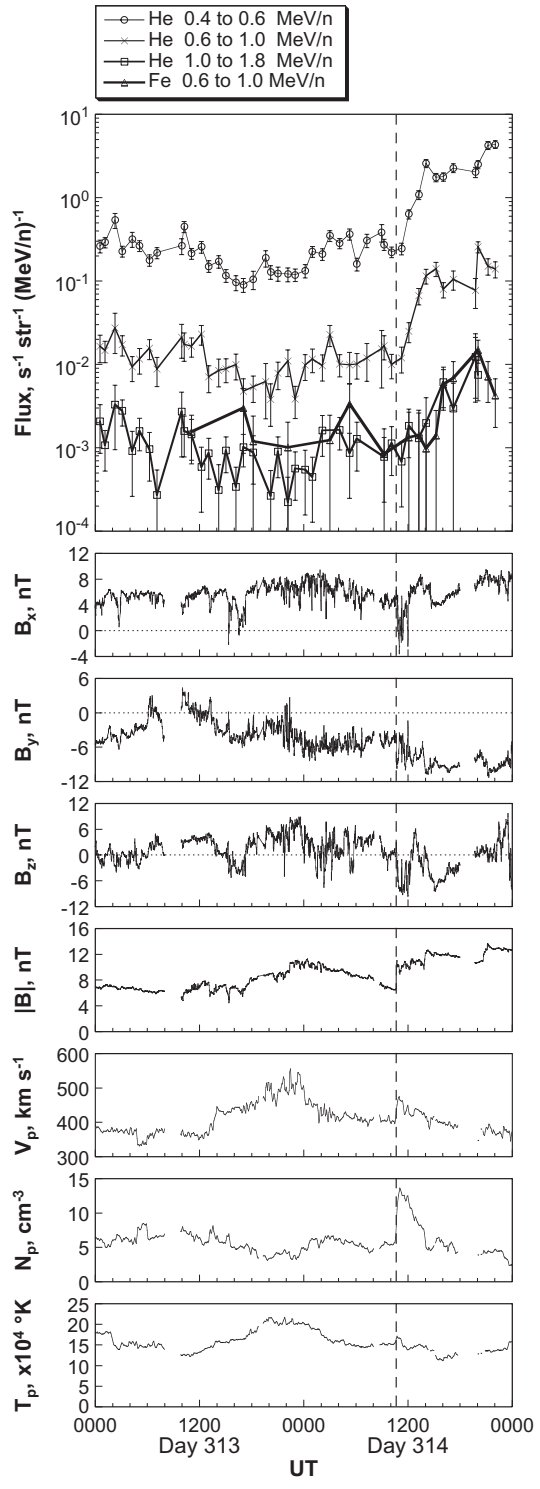

Fig. 5. He (^{3}He+^{4}He) flux, plasma and magnetic field data for the 9 November 1980 event.

of a solar particle event on quiet field lines where the latter have been swept up by the shock. This type of scenario has been previously discussed by Tsurutani et al. (1982) for a CIR field configuration (see their Fig. 6 for an illustration). Another possibility is that the event is due to shock accelera-

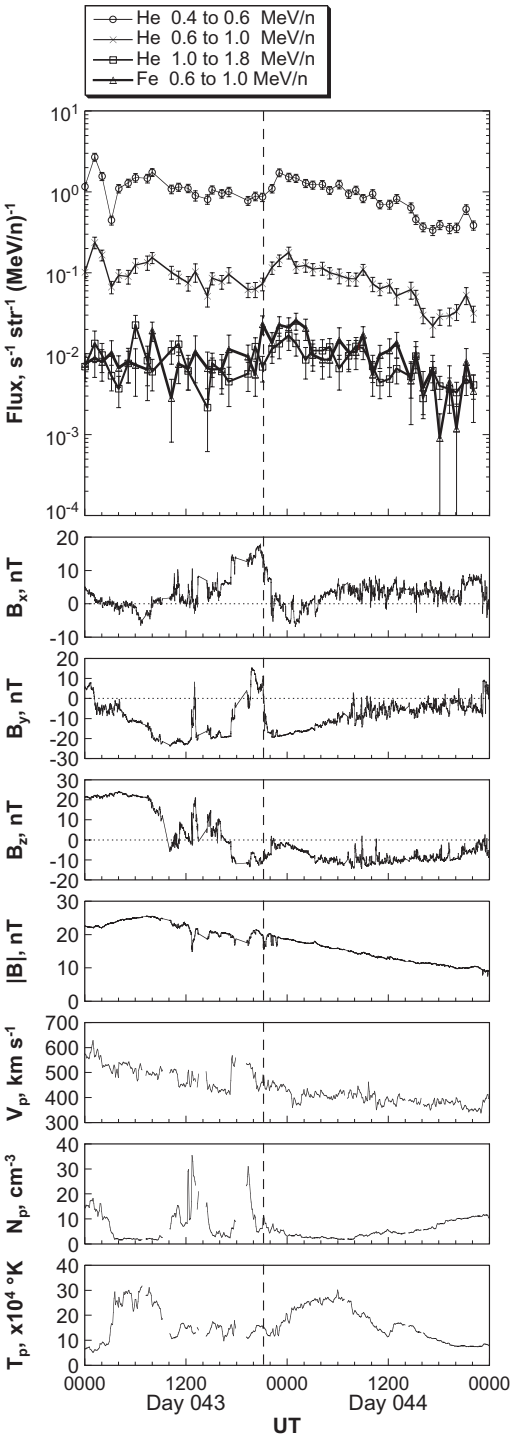

Fig. 6. He (^{3}He+^{4}He) flux, plasma and magnetic field data for the 12 February 1982 event.

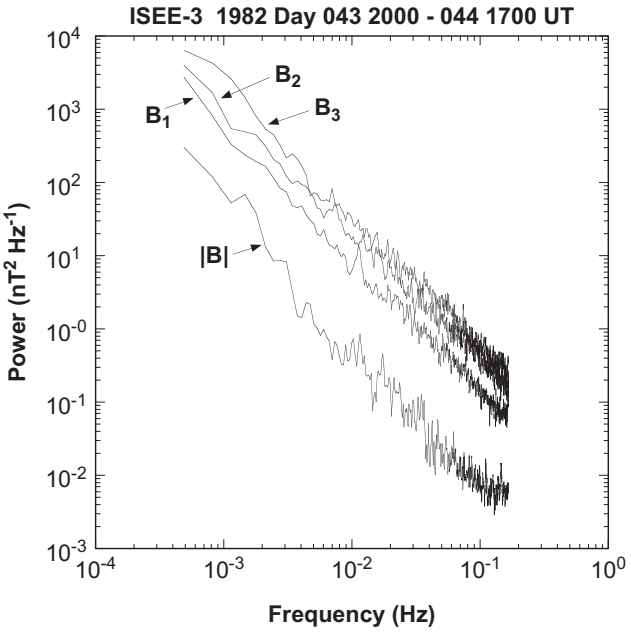

Fig. 7. Magnetic power spectra for the 12 February 1982 event. The two transverse components are indicated by the subscripts 1 and 2.

tion by a quasi-perpendicular shock that had variable normal directions while propagating to 1 AU (thus the lack of particle flux right at the shock surface). Interplanetary shock acceleration of substantial amounts of ^{3}He have recently been observed both in large solar particle events (Mason et al., 1999) and in interplanetary shock events (Desai et al., 2001). The ^{3}He is apparently accelerated (along with solar wind or other suprathermals) when a shock passes through remnants of prior ^{3}He-rich solar particle events, and the chances of this are high during periods of high solar activity. This can lead to ^{3}He/^{4}He values hundreds of times larger than is typical for the solar wind. Mason et al. (1999) found that during the 1998–1999 periods of high sunspot count, ^{3}He was present more than 50% of the time. Since the 9 November 1980 event also took place during sunspot maximum, there is an excellent chance that this mechanism is responsible for the ^{3}He enrichment observed then. For this reason, we have not listed a particle mean free path for this event in Table 1, since it did not originate at the Sun, as our interplanetary propagation model assumes.

The 31 July 1981 event is somewhat similar in that a solar particle event peak intensity is found just at or behind an interplanetary shock. Unfortunately, there is a spacecraft tracking gap right at the shock. The data gap extends from $\sim$05:30 to 14:00 UT, and the particle event onset and field jump is located within the gap. The simultaneous occurrence of the particle event onset and shock unfortunately cannot be determined, as well as whether the particles exhibit dispersion or not. However, the fact that two of the eight He events have this correlation with the shocks seems to be more than coincidental.

The final event of this section, on 12 February 1982, is shown in Figs. 6 and 7. The solar particle event is small in intensity. The event starts at $\sim$20:00 UT, day 43 of 1982. In Fig. 6, one can note that if there is velocity dispersion present, it is very small. We have therefore listed the dispersion of this event as being "questionable" in Table 1. There is a sharp discontinuity in the magnetic field directionality

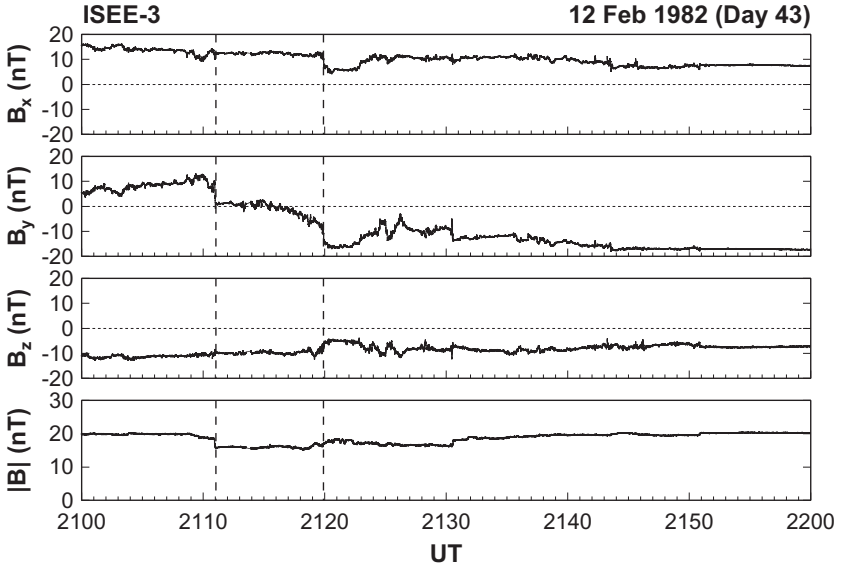

Fig. 8. High-resolution magnetic field data for 12 February 1982. Discontinuities are indicated by the dashed vertical lines.

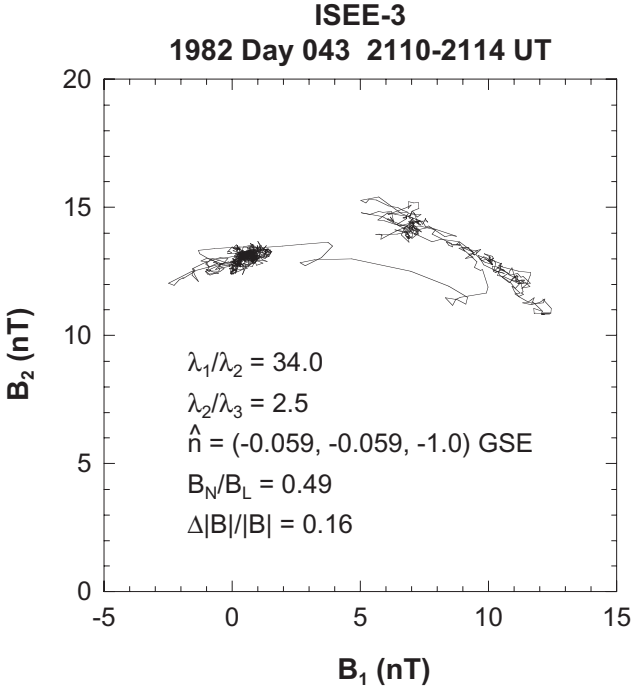

Fig. 9. Minimum variance analysis results for the first discontinuity of Fig. 8. This hodogram displays the field variation in the maximum variance (B_1)-intermediate variance (B_2) plane.

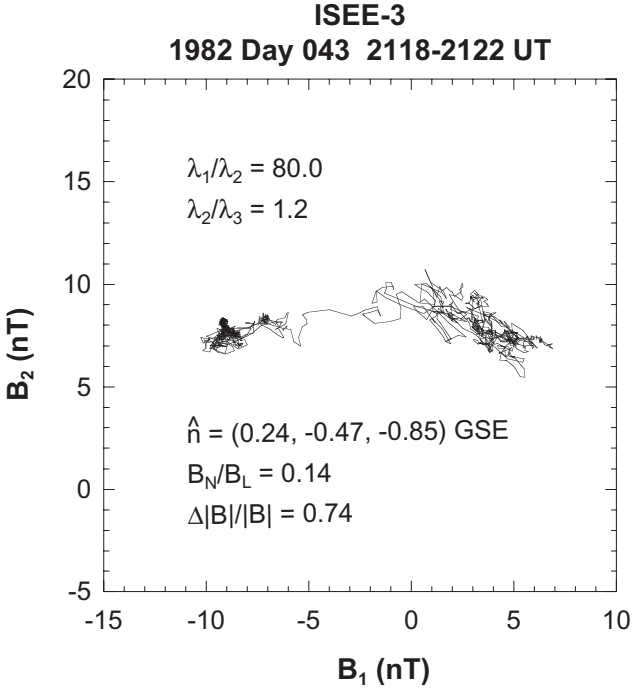

Fig. 10. Minimum variance analysis results for the second discontinuity in Fig. 8. The coordinate definition is the same as that in Fig. 9.

just prior to the peak in the particle flux. This is present near ∼22:00 UT and is denoted by a vertical dashed line. The discontinuity is best observed in the B_x and B_y components. There is a short duration magnetic field magnitude decrease as well. Following the discontinuity, the magnetic field is devoid of large amplitude waves and discontinuities. This is particularly true from 22:00 UT day 43 to 06:00 UT day 44. There are some small amplitude waves present beyond this interval. The high magnetic field magnitude and the lack of waves identify this region as part of a driver gas (more recently called an interplanetary coronal mass ejection, or ICME) of a solar ejecta event (Zwickl et al., 1983; Tsurutani et al., 1988, 1994). The B_y and B_z variations identify this as a magnetic cloud (Klein and Burlaga, 1982; Zhang and Burlaga, 1988) within the ICME.

The magnetic power spectra for the entire particle event, from 20:00 UT day 43 to 17:00 UT day 44 is given in Fig. 7. Again, we note that the power in the transverse compo-

Table 3. Siscoe et al. (1968) standard of IMF active, intermediate and quiet activity

Activity Level	Average transverse power (nT^2/Hz)	Average $\|\boldsymbol{B}\|$ (nT)	Normalized transverse power (Hz^{-1})
active	$8.2 \times 10^{-3} f^{-1.55}$	5.54	$2.67 \times 10^{-4} f^{-1.55}$
intermed.	$4.5 \times 10^{-3} f^{-1.55}$	4.89	$1.88 \times 10^{-4} f^{-1.55}$
quite	$8.5 \times 10^{-4} f^{-1.59}$	2.85	$1.05 \times 10^{-4} f^{-1.59}$

nents are well over an order of magnitude higher than in the compressional component. The transverse wave intensity is $P^2 = 1.1 \times 10^{-2} f^{-1.7}$ nT^2 Hz^{-1}. The average field magnitude is 15.6 nT and the normalized spectra is $4.5 \times 10^{-5} f^{-1.7}$ Hz^{-1}. Thus the normalized field is considerably below the "quiet" interplanetary condition. Even this value is an overestimate of the true transverse wave power, as some of the "power" in the spectrum is due to the field gradients that are present in the magnetic field (see bottom panels of Fig. 8), and not due to waves.

A detailed blowup of the interplanetary discontinuity is given in Fig. 8. Upon closer examination, we find that the field orientation change occurs in two steps (i.e. this appears to be a double discontinuity). The two events occur at $\sim$21:11 and $\sim$21:21 UT and are denoted by vertical dashed lines.

Minumum variance analyses (Sonnerup and Cahill, 1967) were performed on each of these discontinuity events. For discontinuities, we can generally identify the "type" by examining the field along the normal direction and by the field magnitude change across the event (Smith, 1973; Tsurutani et al., 1995; Ho et al., 1995; Tsurutani and Ho, 1999). The discontinuities are plotted in the minimum variance coordinates in Figs. 9 and 10. The maximum, intermediate, and minimum variance directions will be called $\boldsymbol{B}_1$, $\boldsymbol{B}_2$, and $\boldsymbol{B}_3$, respectively.

For the first discontinuity, we have analyzed the interval between 21:10:03 and 21:14:00 UT. The upstream magnetic field magnitude value is 18.8 nT and the downstream value is 15.7 nT. Therefore, $\Delta|B|/|B|$ is 0.16. The field average along the normal direction (0.06, 0.06, 0.99) in GSE coordinates is 9.2 nT. The ratio B_n/B_L is 0.49, where B_n is the field component normal to the discontinuity, and B_L is the larger field magnitude on either side of the discontinuity. The ratios of the eigenvalues are $\lambda_1/\lambda_2 = 34.0$, and $\lambda_2/\lambda_3 = 2.5$, indicating a highly arc-like polarization. In this notation, λ_1, λ_2, and λ_3 correspond to the maximum, intermediate, and minimum eigenvalues of the covariance matrix. A "pure" tangential discontinuity has no normal field across B and a "pure" rotational discontinuity has a B_n/B_L value of 1.0 and no magnitude jump across the surface. The large field magnitude jump across the discontinuity and the moderate normal field component indicate that this event has both tangential and rotational discontinuity properties (Landau and Lifschitz, 1960; Smith, 1973). The hodogram for this discontinuity is given in Fig. 9. For discussion of events that apparently have the properties of both rotational and tangential discontinuities, we refer the reader to Neugebauer et al. (1984, 1986) and Tsurutani et al. (2001).

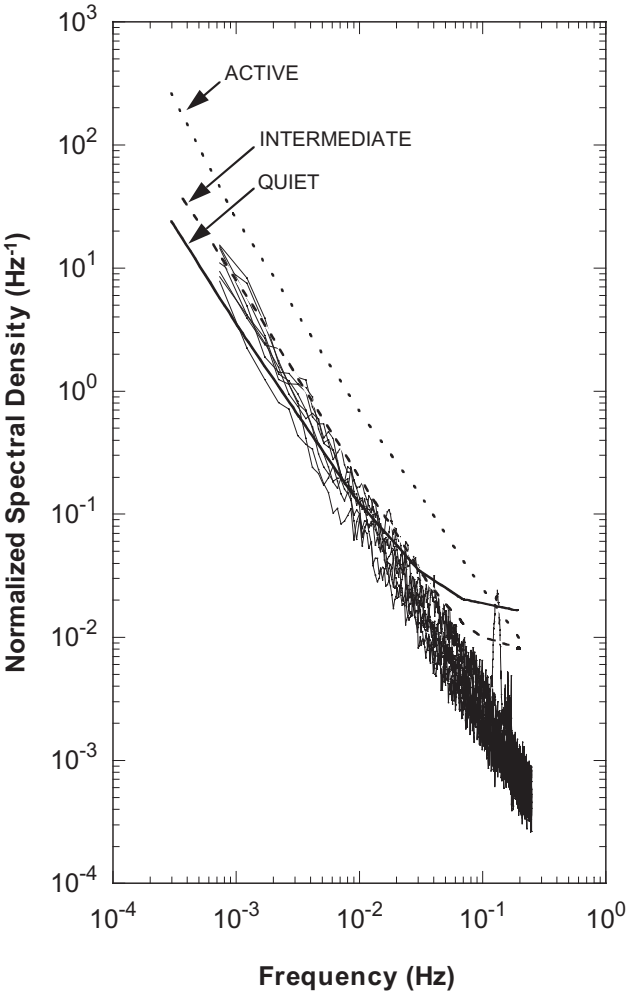

Fig. 11. Comparison of the normalized transverse IMF power spectra for the eight ^{3}He-rich events of Tables 1 and 2 and the normalized Siscoe et al. (1968) classification of the IMF activity level (from Table 3).

The time interval for the second discontinuity, 21:18:00 to 21:22:00 UT, has also been analyzed. The hodogram is shown in Fig. 10. $\Delta|B|/|B|$ is 0.14, B_n/B_L is 0.74, and $\lambda_1/\lambda_2 = \lambda_2/\lambda_3 = 1.2$, again consistent with arc polarization. This discontinuity also has both rotational and tangential discontinuity properties. Clearly, the combination of the two discontinuities have kept the particles reasonably well confined to the interior of the magnetic cloud.

The two discontinuities are quite similar in structure and properties. Both have properties of a rotational and a tangential discontinuity. Structures similar to this have been previously noted at the edges of magnetic clouds/driver gases (Galvin et al., 1987). It has been recently speculated by Tsurutani and Gonzalez (1995) and Tsurutani et al. (1998), that the interval between the two discontinuities correspond to

the "bright outer loops" of a CME (convected to 1 AU). In this scenario, the "dark matter" of a CME corresponds to the low β magnetic cloud that has been discussed by Klein and Burlaga (1982).

The magnetic power spectra for the eight events are given in Table 2, the three columns correspond to: (a) the raw power spectra, (b) the average magnetic field, and (c) the normalized power spectra. The Siscoe et al. (1968) power spectra for "quiet", "intermediate", and "active" periods are listed in Table 3 for comparison. Figure 11 gives a graphical depiction of Tables 2 and 3. The "turn-up" at the highest frequencies of the Siscoe et al. (1968) curves is most likely due to instrument noise.

4.1.1 Scattering mean free paths determined by particle measurements

The scattering mean free paths for the Table 1 events (^{3}He-rich periods) were obtained by comparing the event time/intensity profiles and anisotropies with the predictions of a Boltzmann equation model of interplanetary scattering which includes the effects of particle pitch-angle scattering and adiabatic defocusing as the particles move through magnetic fields of varying strength (Roelof, 1969; Earl, 1974, 1981). Mason et al. (1989) published numerical solutions of this equation based on the technique of Ng and Wong (1979) for observations from the ISEE-3 ULEWAT instrument for nominal values of the solar wind speed. We use these solutions here to estimate the scattering mean free paths for the Table 1 events which were not previously fitted. The results are given in Table 1.

For the ^{3}He-rich events, the most distinctive features of the particle fluxes are the "pulse/wake" ratio (the ratio of the maximum flux to the flux in the post maximum interval), and the anisotropy. While all events show very large forward/backward flux ratios, the ratio of the forward moving particle flux (pitch angle cosine $\mu = 1.0$) to those with $\mu = 0$ is a sensitive function of the scattering mean free path. For interplanetary mean free paths of 0.5, 1.0, and 3.0 AU, the respective pulse/wake ratios are approximately 3, 10, and 100 (Mason et al., 1989). For the same set of mean free paths, the ratio of the $\mu = 0.1$ to $\mu = 1.0$ fluxes at maximum intensity is, repectively, ~ 0.3, ~ 0.1, and ~ 0.01. These typical values make it possible to estimate the mean free paths in Table 1. As a practical matter, however, other factors may come into play. If, for example, the ^{3}He-rich event occurs when the He interplanetary fluxes are already enhanced due to another flare or a shock, there will be a background isotropic particle population that will tend to mask the event anisotropies. Similarly, if the interplanetary magnetic field fluctuates out of the ecliptic plane during the interval of anisotropy determination, then the fluctuations will smear out the anisotropy. Finally, if the event is very small, the ability to measure large peak/wake or anisotropy ratios will be limited by statistics. It is important to realize that all of these limiting aspects of the data all lead to a mean free path determination that is less than the true value. Therefore, the mean free paths in the table should be assumed to be lower limits.

4.1.2 Resonant wave-particle interaction calculation of mean free paths using IMF power spectra

The particle pitch angle diffusion coefficient (i.e. pitch angle scattering rate) can be derived using physical arguments following that of Kennel and Petschek (1966) and Tsurutani and Lakhina (1997). The condition of cyclotron resonance between the waves and the particles can be written as

$$\omega - k_{||} V_{||} = n\Omega_i, n = 0, \pm 1, \pm 2, \ldots \quad (1)$$

In the equation above, ω and $\boldsymbol{k}$ are the wave frequency and wave vector, Ω_i is the ion cyclotron frequency in ambient magnetic field. The particle velocity $V_{||}$ is assumed to be the velocity of the guiding center motion; its direction is along the ambient magnetic field line and its magnitude is $V = \mu V_0$, where μ is the cosine of the particle pitch angle and V_0 is the particle velocity magnitude. The angular distribution of wave vector $\boldsymbol{k}$ is assumed to be a forward hemisphere centering in the direction of $V_{||}$. The observation of the propagation directions of solar wind rotational discontinuities reported by Tsurutani et al. (1996) (see also Tsurutani and Ho, 1999) has shaped our choice for the above assumption, In addition, this assumption also appears to agree with some recent work on the predominance of quasi-perpendicular turbulence versus quasi-parallel turbulence (Bieber et al., 1996).

For Alfvén waves propagating in the solar wind plasma frame, the phase velocity is V_A. In the spacecraft frame however, we have

$$\omega = 2\pi f = |\boldsymbol{k}| \cdot (V_{SW} \cos\psi + V_A \cos\gamma), \quad (2)$$

in which γ is the angle between the stationary plasma frame Alfvén wave vector and the radial direction, and ψ is the angle between $\boldsymbol{k}$ and $\boldsymbol{V}_{SW}$. Considering that near 1 AU the Alfvén speed is about a tenth (i.e. negligible) of the solar wind speed, the Alfvén speed contribution in Eq. (2) is negligible. Taking the angle between $\boldsymbol{k}$ and $\boldsymbol{V}$ to be θ, Eq. (1) now becomes

$$2\pi f = \left(1 - \frac{\mu V_0}{V_{SW} \cos\psi} \cos\theta\right) = n\Omega_i . \quad (3)$$

If the particles of interest are He^{++} and 0.4 MeV / nucleon energy, $V_0 = 8.8 \times 10^8$ cm s^{-1} is much larger than the solar wind speed V_{SW}. For normal interplanetary wave spectral distributions, the primary resonance in Eq. (3) occurs at $n = -1$ because $\cos\theta$ is always positive in this discussion (we do not consider the $n = 0$ term (transit time damping: Schlickeiser and Miller, 1998) because a much lower compressional power is shown in this paper and the lack of knowledge of whether that this power represents magnetosonic waves or not). In this case the ions are resonant with right-hand polarized waves; therefore, in the final estimate of mean free paths, the effective wave transverse power should be $(P_1 + P_2)/2$, where 1 and 2 indicate the two transverse

Table 4. Mean free paths for 1 MeV/nuc ^{3}He ions of the ^{3}He-rich scatter-free events ($V_{He} = 1.385 \times 10^9$ cm/s)

Event	B_0 (nT)	$\Omega_{^3He^{++}}$ (rad s^{-1})	P transverse (nT^2/Hz)	D (s^{-1})	* λ_{W-P} (AU)	* λ_{He} (AU)
1	6.30	0.402	$3.26 \times 10^{-3} f^{-1.7}$	1.03×10^{-3}	0.09	1.0
2	8.11	0.517	$2.81 \times 10^{-3} f^{-1.7}$	5.77×10^{-4}	0.16	1.0
3	4.63	0.295	$6.58 \times 10^{-3} f^{-1.8}$	6.05×10^{-4}	0.15	0.5
4	9.93	0.634	$7.43 \times 10^{-3} f^{-1.7}$	1.08×10^{-3}	0.08	2.0
5	6.25	0.399	$1.89 \times 10^{-3} f^{-1.7}$	6.05×10^{-4}	0.15	0.5
6	11.47	0.732	$4.82 \times 10^{-3} f^{-1.7}$	5.49×10^{-4}	0.17	0.3
7	9.66	0.616	$3.60 \times 10^{-3} f^{-1.6}$	3.45×10^{-4}	0.27	0.5
8	15.56	0.993	$1.08 \times 10^{-3} f^{-1.7}$	7.33×10^{-4}	0.13	0.5

* λ_{W-P} is the wave-particle interaction estimates of mean free paths at 1 AU.
λ_{He} is the observational value of mean free path determined from particle intensities and anisotropies.

directions of the ambient field. The wave resonant frequency is stated as

$$f_{res} = \left(\frac{f^{++}}{\frac{\mu V_0}{V_{SW}\cos\psi}\cos\theta - 1} \right),$$
$$f^{++} = \frac{\Omega^{++}}{2\pi} = \frac{qB_0}{2\pi mc}. \quad (4)$$

Following Eq. (3.9) of Kennel and Petschek (1966), the pitch angle scattering rate for a given resonant velocity due to interactions with waves in a wave-number band of width Δk about resonance is

$$D = \frac{(\Omega^{++})^2}{2\pi} \cdot \frac{V_{SW}\cos\psi}{\mu V_0 \cos\theta} \cdot \frac{P_{res}}{B_0^2},$$
$$P_{res} = \left.\frac{(B\prime)^2}{\Delta f}\right|_{res}, \Delta f = \frac{1}{2\pi}\Delta k \cdot V_{SW}, \quad (5)$$

where $B\prime$ is the wave amplitude in either the left-handed or right-handed waves that are in resonance with the particle, P_{res} is the wave energy per unit Hz evaluated at the resonant frequency and is related to the two observed transverse power spectra $P_{res} = (P_1 + P_2)/2$. Assume that the wave power spectra have a power spectral index of α, that is, $P_{res} = A f_{res}^{-\alpha}$ and $\mu V_0 \cos\theta \gg V_{SW}\cos psi$, the effect of averaging over the θ and ψ angles is (see Appendix A)

$$\langle D\rangle_\theta \approx \left.\frac{1.1}{\alpha}\cdot D\right|_{\theta=0}$$
$$= \frac{\left(\Omega^{++}\right)^2}{2\pi}\frac{1}{B_0^2}\frac{1.1}{\alpha}A\left(f^{++}\right)^{-\alpha}\left(\frac{\mu V_0}{V_{SW}}\right)^{\alpha-1}. \quad (6)$$

Further averaging over the cosine of the particle pitch angle results in

$$\langle D\rangle_{\theta,\mu} = \frac{1.1}{\alpha^2}\frac{\left(\Omega^{++}\right)^2}{2\pi}\frac{V_{SW}}{V_0}\frac{1}{B_0^2}A\left(\frac{V_{SW}f^{++}}{V_0}\right)^{-\alpha}. \quad (7)$$

The time for scattering one radian in pitch angle T is $\sim 1/D$, and the particle mean free path is $\lambda_{W-P} = TV_{He}$, where λ_{W-P} is the wave-particle interaction estimate of the mean free path. Equation 7 is used for estimating the mean free paths λ_{W-P} in Table 4 of ^{3}He-rich events.

We note that the formalism used in the pitch angle scattering calculations differs slightly from that of Schlickeiser and Miller (1998), who have considered higher order cyclotron resonance plus the transit time damping ($n = 0$) term. We have considered only the first order term ($n = -1$). Use of higher order cyclotron resonance terms is more theoretically complete, but should only change the results slightly. The wave power is considerably less at higher frequencies due to the power law spectrum of the waves (therefore also the higher order resonance terms). Transit time damping was not included in our calculations because there was no clear evidence that the compressional field power represents magnetosonic waves (also the wave power is 30 times lower than the power in the transverse field fluctuations). Rather tangential discontinuities (Ho et al., 1995) and "magnetic decreases" (Tsurutani and Ho, 1999; Tsurutani et al., 2000) convected by the solar wind past the spacecraft may represent a substantial portion of this compressional power.

4.2 Intense solar proton events

We have analyzed intense solar flare proton events to determine if there is the possibility of self-generated waves present at 1 AU (Reames, 1989; Ng and Reames, 1994). Reames and Ng (1998) believe that they have detected an energetic proton "streaming limit", due to wave-particle scattering. The seven proton events analyzed are listed in Table 5.

An example of observations during an intense event is shown in Fig. 12. The format is the same as that of Fig. 2, with the proton (and Helium) data in the top panel and the magnetic field in the bottom four panels. An interplanetary shock is denoted by a dashed vertical line. The 12.0 to 19.0 MeV/nucleon proton peak occurs right at the shock, indicating that this particle event is most likely due to local shock acceleration (McDonald et al., 1976; Pesses et al., 1982; Forman and Webb, 1985). It is known that the particle anisotropies caused by this local acceleration lead to elec-

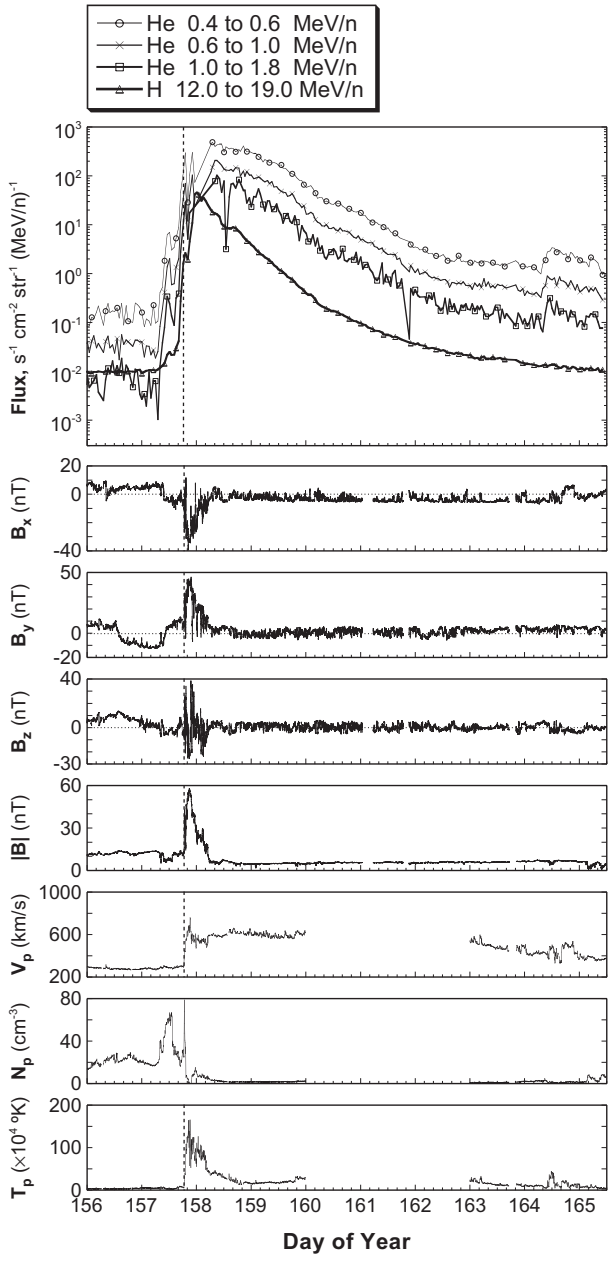

Fig. 12. A high flux energetic 12 to 19 MeV proton event, associated with an interplanetary shock (vertical dashed line), on day 157, 1979.

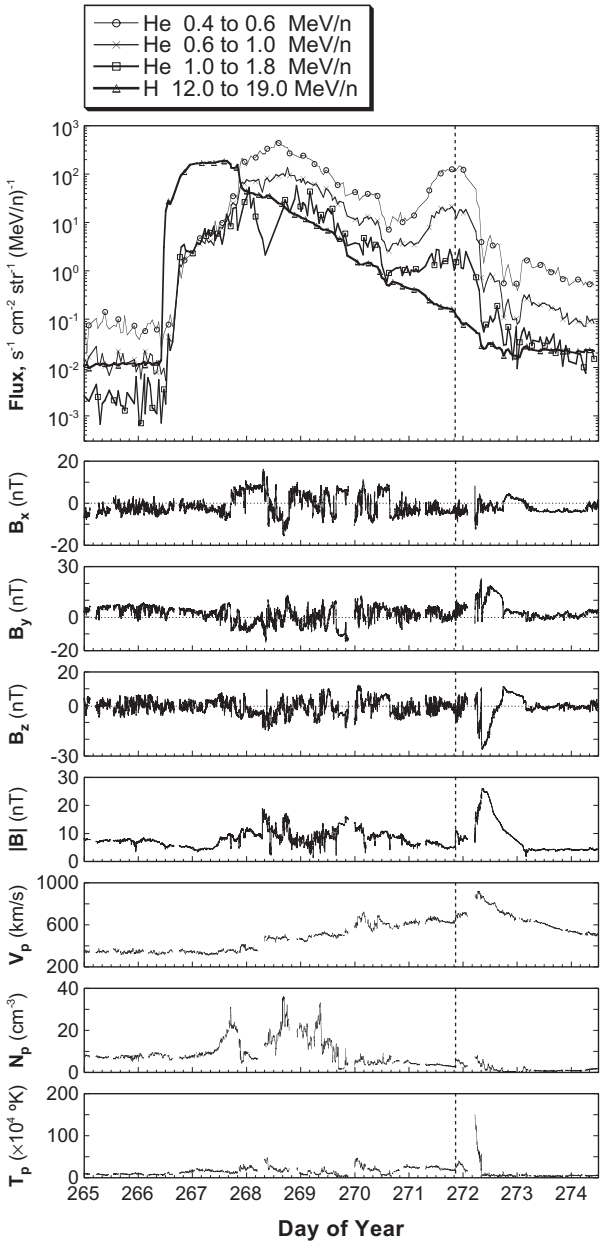

Fig. 13. Energetic particle fluxes, magnetic fields and solar wind plasma data for the 23–26 September 1978 event. This particle event occurs well away from any strong interplanetary disturbances.

tromagnetic wave generation (Tsurutani et al., 1983), thus waves would be expected in the foreshock region. In our search for proton event wave generation we excluded such regions.

Figure 13 shows a "clean" solar proton event, one that occurs well away from interplanetary shocks. At the leading edge of the event, $\sim$ day 267, the 12.0 to 19.0 MeV/nucleon proton peak flux is $\sim 2\times10^2$ cts s^{-1} str^{-1} (MeV/nucleon)$^{-1}$. The flux for low energy 0.6 to 1.0 MeV/nucleon protons would be expected to be orders of magnitude higher. One estimation would be to take the 0.6 to 1.0 MeV/nucleon He flux and increase it by 60 times (Mason et al., 1980; Mazur et al., 1993), also with the nucleon number factor 0.4, 60 (on day 268) $\times 60 \times 0.4 = 1.4 \times 10^3$ cts s^{-1} str^{-1}.

The proton event had a long duration, starting on 23 September and continuing into 2 October, lasting more than nine days. This is fairly typical. Also note that the He particles did not have a profile of a fast rise followed by a slow decay that was present in the (shock acceleration) event of Fig. 12.

Assuming the extrapolated peak flux of $\sim$ 0.6 MeV protons to be 1.4×10^3 cts s^{-1} str^{-1}, we obtain a beam (over

2π str) energy density of 5.3 eV cm^{-3}. For a solar wind thermal plasma density of 5 ions cm^{-3} and a temperature of $\sim 10^5$ K, the solar wind thermal plasma energy density is 50 eV cm^{-3}. The Alfvén speed V_A in the solar wind at 1 AU is ~ 70 km s^{-1}. The flow of energetic protons through the ambient plasma can be thought of as a beam. The ratio of the velocity of 0.6 MeV protons to the Alfvén speed is ~ 150. The Gary et al. (1985) criteria for beam instability is nearly satisfied for this event. Gary et al. (1985) required a minimum beam energy density of 14% and a high $V_b/V_A > 10$ ratio. Here the former ratio is 11% and $V_b/V_A \approx 150$. Thus this particle beam is marginally stable.

There are two prime regions of an energetic particle event where self-generated waves may occur. The leading edge, where the particles are most field-aligned (and beamed), is one possible region. The anisotropy will be conducive to the resonant ion beam instability (Gary et al., 1985; Tsurutani, 1991). A second region is near the location of the peak flux. If the particle fluxes are sufficiently intense, a nonresonant (firehose) instability may occur (Sentman et al., 1981).

The search for both resonant and nonresonant waves was conducted. We did not find any waves (at 1 AU) that could obviously be associated with the energetic particle events. These observations are in general agreement with the results of Valdes-Galicia and Alexander (1997) and Alexander and Valdes-Galicia (1998), in a search for waves in the region 0.3 to 1.0 AU.

All of the other intervals listed in Table 5 were examined using high time resolution field data. The search for self-generated waves was not fruitful. An upper limit to the self-generated waves by energetic proton events is 10^{-3} nT^2 Hz^{-1}.

The energy density of the beam was noted to be a substantial fraction of the ambient plasma thermal energy density and the beam was found to be marginally stable. It is possible that the beam had become unstable, and waves were generated scattering the beam and dropping it below the instability criteria. However, if this scenario is the correct one, the corresponding waves were not detected. Another possibility is that the particle event had intensities just under the instability limit. One should search for even greater proton events at 1 AU to resolve this issue.

Many of these high flux events were associated with local interplanetary shocks. A good example is shown in Fig. 13. The particle onset occurs slightly upstream of the shock, but the peak fluxes in all energy channels are in the postshock region. This is consistent with the recent picture of the important role that interplanetary shock acceleration plays in "solar" events (Tsurutani et al., 1982; Sanahuja et al., 1995).

The importance of interplanetary shock acceleration was noted in several other events as well. The peak particle fluxes were correlated with shocks for the 20 August 1979, 26 April 1981, and 17 May 1981 events.

5 Summary of observations

1. Low intensity He events that had clear velocity dispersion were found to be typically associated with quiet to intermediate interplanetary magnetic field activities (i.e. the field fluctuations are low relative to typical levels). These particle events occurred well away from high speed streams or from strongly Alfvénic wave intervals (Belcher and Davis, 1971; Zwickl et al., 1978; Tsurutani et al., 1994; Mazur et al., 1996), regions where pitch angle scattering rates would be expected to be high. The reasons for this correlation are unclear at the present time. One possibility is that if more waves were present along the particle path, the scattering would be more intense and the events more difficult or impossible to identify at 1 AU. Another possibility is that the ^{3}He-rich event occurs preferentially near quiet regions at the Sun.

2. Of the ^{3}He-rich events (those not discussed in point 1) taken from the list of Kahler et al. (1985) that did not have clear velocity dispersion, one was associated with an interplanetary shock, and another with a magnetic cloud. For the shock-related events, the particles are most likely due to (local) interplanetary shock acceleration of ^{3}He remnants from earlier impulsive particle events (see Mason et al., 1999; Desai et al., 2001). The particle event that was in a magnetic cloud occurred on very smooth magnetic field lines (see also Mazur et al., 1998). The ICME was bounded by a pair of discontinuities. Clearly, the pair of discontinuities contained the energetic particles to propagate with the structures, and no velocity dispersion was possible.

3. Large solar proton events were examined for the presence of self-generated waves at both the leading edge and at the peak flux regions. No obvious self-generated waves were found to a limit of 10^{-3} nT^2 Hz^{-1}. This result is in agreement with the results of the Alexander and Valdes-Galicia (1998) study done at closer heliocentric distances (0.3 to 1.0 AU). Our present study indicates that the proton 0.6 to 1.0 MeV events were only marginally stable. Thus waves may have been generated at other distances from the Sun, then they scattered the particles, and reduced the flux to the marginally stability limit. A search for even greater flux events at 1 AU and concurrent waves could answer this question.

4. The same He event time intensity profiles and front-to-back anisotropies have been used to derive scattering mean free paths λ_{He}. This method has been documented in Mason et al. (1989). The values of λ_{He} found for the He events range from 0.3 to 2.0 AU.

5. We use an improved wave-particle scattering calculation that includes wave polarization, measured wave normal vector distribution and in-situ transverse wave spectra. For the eight He-rich events, improved calculations of scattering mean free paths λ_{W-P} are performed. The λ_{W-P} values are generally smaller than

Table 5. High-intensity solar particle events

Event	Dates	Event onset		Importance	Location	Radio bursts		
		Day	Hα Time (UT)			II	III	IV
1	23–26 Sep 1978	266	09:44	3B	N35 W40	X	X	X
2	6–8 Jun 1979	157	∼ 04:55	2B	N14 E14	X		X
3	19–22 Aug 1979	231	14:21	SB	N08 E90	X	X	X
4	15–21 Sep 1979	258	∼ 07:00	–	N07 ∼E107	X		X
5	24–26 Apr 1981	114	∼ 13:44	2B	N18 W50	X	X	X
6	9–12 May 1981	129	∼ 22:01	2B	N09 E37	X		X
7	16–18 May 1981	136	07:53	3B	N11 E14	X		X

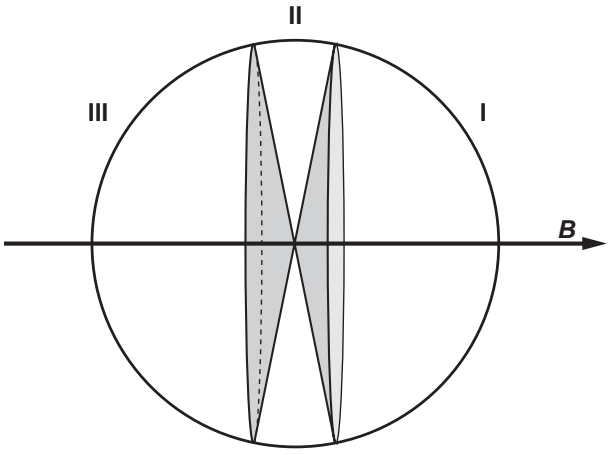

Fig. 14. Illustration of the three pitch angle scattering regions. I is the forward hemisphere of less than 90° pitch angles, and II is the narrow region near 90°, where resonant (small amplitude) wave-particle interactions do not take place. Region III is the backward propagating (sunward) pitch angles.

the empirical λ_{He} mentioned above. The ratio of $\lambda_{W-P}/\lambda He$ has a range from 0.04 to 0.63 and the average of λ_{W-P} is 0.15 AU. Our current calculation differs from ion observations modelling by a factor of ~ 5 on the average for 1 MeV/nucleon Helium ions.

6 Discussion of ^{3}He results

Although wave polarizations, wave normal distributions and in-situ transverse power spectra were included in this study, there are still substantial differences between the calculated λ_{W-P} and λ_{He} values. Previous works (e.g. reviews by Palmer, 1982; Tan and Mason, 1993) have noted even greater discrepancies.

To understand what we have calculated in the two values λ_{W-P} and λ_{He}, we use Fig. 14 to schematically illustrate three different regimes of particle pitch angle scattering. The pitch angles range from 0° (along $\boldsymbol{B}$) to 180° (antiparallel to $\boldsymbol{B}$). Particles in Region I are propagating anti-sunward, in Region II the particles have near 90° pitch angles (Region II illustrates the area between the two cones of pitch angles, one centered at 0° and the other at 180°), and in Region III the particles are propagating backward toward the Sun.

λ_{W-P} is conventionally calculated as the pitch angle scattering rate and represents diffusion by ~ 1 radian in Region I. Scattering across 90° (or the lack thereof) in Region II is not appreciable for these types of interactions. We know from quasi-linear theory that interaction at 90° pitch angle is zero (see Eq. 1), i.e. diffusion cannot occur at exactly 90°. Examples of this can be found in magnetospheric storm particle measurements (Lyons et al., 1972), where the particle distributions are highly peaked at 90° ($\sin^n \alpha$, $n = 5 \sim 10$). We have considered the diffusion rate in Region III (by anomalous cyclotron resonance) and find that it is essentially the same as in Region I (the details of this calculation are relatively simple and are not shown here to save space).

λ_{He}, on the other hand, is the diffusion rate from Region I through Region II to Region III. If diffusion through Region II is the slowest, the value of λ_{He} is predominantly determined by the diffusion through this region. Thus we note that there should not be a direct correspondence between λ_{He} and λ_{W-P}, unless the pitch angle diffusion rates in all three regions are somehow equal. The fact that λ_{He} is much larger than λ_{W-P} may indicate that the diffusion in the three regions are indeed unequal. From the above arguments, it would be expected that scattering through Region II would be the slowest. This may be an explanation for the different λ_{W-P} and λ_{He} values.

In order to further examine the above argument, we performed a test particle simulation, in which ion orbits are integrated in time under the influence of static magnetic field turbulence, which is given as a superposition of parallel, circularly polarized Alfvén waves with equal propagation velocities (slab model). In this model, the ion energy in the wave rest frame is constant, thus there is no energy diffusion of ions. Both right- and left-hand polarized waves are included, although each mode represents a non-compressional superposition of the waves and yields ponderomotive compressional fields, which may act to mirror-reflect the ions. In the simulation, we assumed that the distribution of wave power is given by a power-law distribution with a spectral index γ when $k_{\min} < k < k_{\max}$, and zero otherwise, where k, $k_{\min}$, and $k_{\max}$ are, respectively, the wave number, and the

minimum and maximum wave numbers included in the simulation. The wave phases are assumed to be random.

Figure 15 shows the time evolution of distribution of ion pitch angle cosine, μ, defined as an inner product of the unit vectors parallel to the ion velocity and the magnetic field, in the wave rest frame. For each panel, the horizontal axis represents the initial distribution, $\mu(0)$, and the vertical axis denotes the distribution at some later times, $\mu(T)$, with (a) $T = 40$, (b) $T = 640$ and (c) $T = 10\,240$. Each dot represents a single test particle. Parameters used are: the ion velocity, $v = 10$, $\gamma = 1.5$, $k_{\min} = 6.13 \times 10^{-3}$, $k_{\max} = 3.14$, and the variance of the normalized perpendicular magnetic field fluctuations, $< B_\perp^2 >= 4 \times 10^{-4}$. The number of particles used in the run is 10 000. In the above, all the physical variables have been normalized using the normal (constant) magnetic field, B_0, ion gyrofrequency, and the Alfvén velocity, both defined by using B_0. Note that the resonant wave number for zero pitch angle, $1/v = 0.1$, is within the range of ($k_{\min}$, $k_{\max}$), and that the minimum of $|\mu|$, corresponding to the minimum pitch angle cosine of ions which can resonate with waves, $1/(k_{\max} v) = 0.032$, is sufficiently close to zero.

At $T = 40$, the distribution of μ has not evolved much, and so the dots are almost aligned along the diagonal line in panel (a). Later at $T = 640$, pitch angle diffusion is more evident, represented by a thickening of the diagonal line (panel b). It is also clear that the diffusion is absent in essentially two regimes, $\mu \approx 0$ and $|\mu| \approx 1$. The former is due to the lack of waves which resonate with near 90° pitch angle ions. And the latter is due to geometry, i.e. the Jacobian, which appears as the pitch angle is transformed to its cosine, then vanishes at $|\mu| = 1$, showing that a small deviation of the pitch angle from an exactly parallel direction does not give rise to a deviation of μ at the same order. We also find that the pitch angle diffusion time scale under this particular parameter set is of the order of 1000, by determining that the ions initially around $\mu(0) = 0.5$ are pitch angle scattered to have a width of $\mu(T) \sim 0.3 - 0.4$ at $T = 640$. Panel (c) shows the distribution at $T = 10\,240$, substantially longer than the pitch angle diffusion time scale. Clearly, the majority of the ions stay within the hemisphere they belonged to initially. This is due to the small turbulence energy used in this particular run. However, we should also note that a few ions did escape into the opposite hemisphere, presumably due to a mirror reflection by the compressional field. More detailed analysis on test particle simulations will be reported in a forthcoming paper, which will include discussions of diffusion properties as turbulence energy and the wave phase correlation (Kuramitsu and Hada, 2000) are varied, as well as a comparison of several physical processes which enable the ions to cross the 90° pitch angle.

What is the physical process of scattering particles across a 90° pitch angle? The presence of large amplitude waves with $\delta \boldsymbol{B}/B_0 \sim 1$ could lead to large, single-encounter pitch angle scattering across 90° (see Yoon et al., 1991). This is a resonant interaction process, but this process involves large amplitude waves and is not included in the present quasi-linear theories. A second process is particle mirroring via interaction with $|\boldsymbol{B}|$ variations (see Ragot, 1999, 2000). Random superposition of small amplitude waves may produce

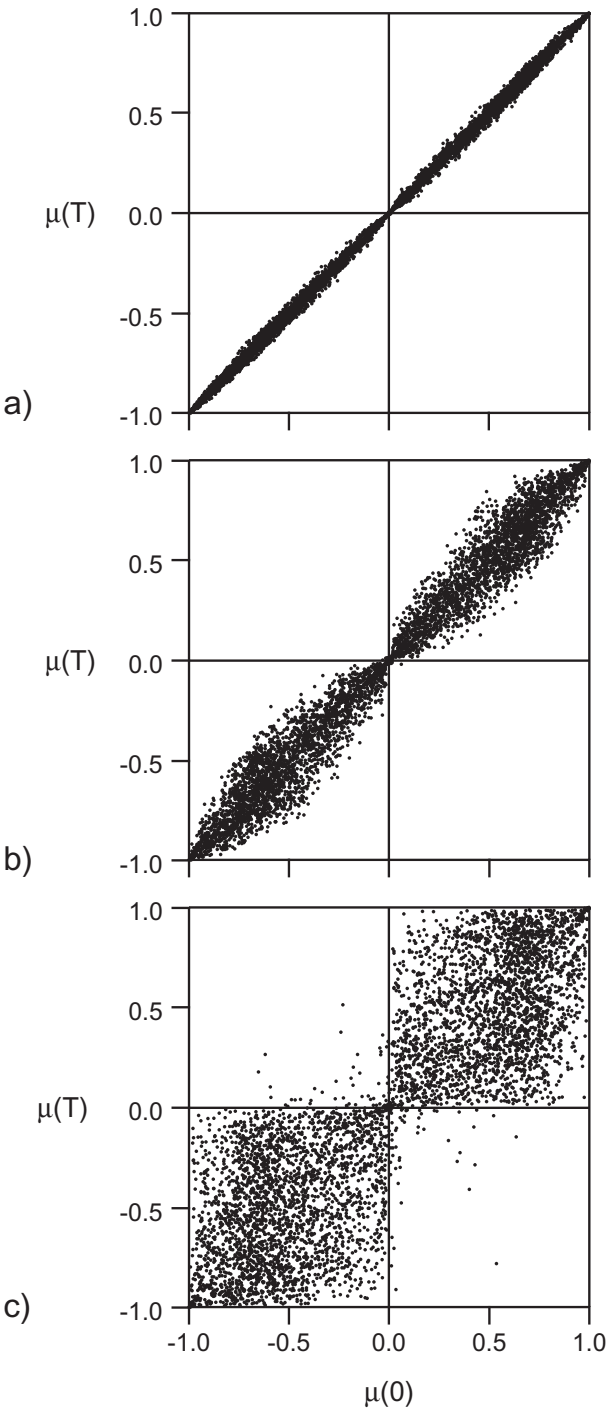

Fig. 15. Particle-In-Cell simulation of time evolution of distribution of ion pitch angle cosine, μ. For each panel, the horizontal axis represents the initial distribution, $\mu(0)$, and the vertical axis denotes the distribution at a later time T. The three panels **(a)**, **(b)** and **(c)** show the distribution at time $T = 40$, 640 and 10 240, respectively. A lack of scattering across 90° pitch angle is evident from the simulation. See text for more details of the simulation parameters.

the $|\boldsymbol{B}|$ power spectra shown in Figs. 3 and 7, and lead to mirroring across 90°. Computer simulations using particle-in-cell (PIC) codes should be useful to determine the relative effectiveness of the above two processes. Analytical expressions could then be derived which could be used to modify the Fokker-Plank transport coefficients.

7 Note added in proof

It has recently been found that localized decreases in the interplanetary magnetic field magnitude called magnetic holes (MHs) and magnetic decreases (MDs) are integral parts of nonlinear Alfvén waves. These MHs and MDs should contribute significantly to the interplanetary compressional power. Particle interactions with MHs and MDs may be an effective source of pitch angle scattering through 90°.

Appendix A

Integral over angle θ and ψ

We consider the effect of averaging over the hemispherical $\boldsymbol{k}$ directions to be equivalent to averaging over angles θ and ψ, i.e. is to obtain the factor

$$A(\alpha) = \int \left(\frac{\cos\theta}{\cos\psi}\right)^{\alpha-1} \tag{A1}$$

in a x-y-z cartesian coordinate system, take the z axis to be the radial V_{SW} direction, and x-z plane to be the heliosphere equatorial plane. At 1 AU the ambient field $\boldsymbol{B}_0$ lies in the x-z plane and makes 45° to both the x and z axis. In this frame, the angle between $\boldsymbol{k}$ and $\boldsymbol{B}_0$ is θ, and the angle between $\boldsymbol{k}$ and z is ψ. Let the angle between the x axis and the projection of $\boldsymbol{k}$ onto the x-y plane to be β. The following relation holds at 1 AU:

$$\cos\theta = \frac{\sqrt{2}}{2}\left(\sin\psi\cos\beta + \cos\psi\right). \tag{A2}$$

The averaging over the hemispherical $\boldsymbol{k}$ direction is equivalent to taking the following integral over β and ψ:

$$A(\alpha) = \frac{1}{2\pi}\int_0^{2\pi} d\beta \left(\frac{\sqrt{2}}{2}\frac{\sin\psi\cos\beta + \cos\psi}{\cos\psi}\right)^{\alpha-1}. \tag{A3}$$

It is easier to consider two limiting cases of α values. When $\alpha = 1$, $A(\alpha) = 1$, and $\alpha = 2$, $A(\alpha) \sim 0.7$. In the interplanetary space, we do not expect the factor $A(\alpha)$ to be a rapidly varying function with respect to the power spectral index α. Therefore, we interpolate the value of $A(\alpha)$ between $\alpha = 1$ and 2 for a realistic value of $\alpha = 1.6$. And we conveniently express $A(\alpha)$ as

$$A(\alpha) \cong 0.8 = \frac{1.1}{\alpha}. \tag{A4}$$

Acknowledgement. We wish to thank F. Jones for very helpful scientific discussions. Portions of this work were performed at the Jet Propulsion Laboratory, California Institute of Technology under contract with the National Aeronautics and Space Administration, and at the University of Maryland supported by NASA grant NAGW – 728 and NSF grant ATM-90-23414. G. S. Lakhina thanks the National Research Council for the 1997-1998 award of a Senior Resident Research Associateship at NASA/Jet Propulsion Laboratory.

References

Alexander, P. and Valdes-Galicia, J. F.: A further search on waves generated by solar energetic protons, Solar Phys., 183, 407, 1998.

Balogh, A., Smith, E. J., Tsurutani, B. T., Southwood, D. J., Forsyth, R. J., and Horbury, T. S.: The heliospheric magnetic field over the south polar region of the Sun, Science, 268, 1007, 1995.

Bavassano, B. and Bruno, R.: Solar wind fluctuations at large scale: a comparison between low and high solar activity conditions, J. Geophys. Res., 96, 1737, 1991.

Beeck, J., Mason, G. M., Hamilton, D. C., Wibberenz, G., Kunow, H., Hovestadt, D., and Klecker, B.: A multi-spacecraft study of the injection and transport of solar energetic particles, Astrophys. J., 322, 1052, 1987.

Beeck, J., Mason, G. M., Marsden, R. G., Hamilton, D. C., and Sanderson, T. R.: Injection and diffusive transport of suprathermal through energetic solar flare protons (35 keV–20 MeV), J. Geophys. Res., 95, 10279, 1990.

Belcher, J. W. and Davis, Jr., L.: Large amplitude Alfvén waves in the interplanetary medium, 2, J. Geophys. Res., 76, 3534, 1971.

Bieber, J. W., Wanner, W., and Matthaeus, W. H.: Dominant two-dimensional solar wind turbulence with implications for cosmic ray transport, J. Geophys. Res., 101, 2511, 1996.

Coleman, P. J.: Turbulence, viscosity and dissipation in the solar wind plasma, Astrophys. J., 153, 371, 1968.

Desai, M. I., Mason, G. M., Dwyer, J. R., Masur, M. E., Smith, C. W., and Skoug, R. M.: Acceleration of 3He nuclei at interplanetary shocks, Astrophys. J. Lett., submitted, Feburary 2001.

Earl, J. A.: Coherent propagation of charged-particle bunches in random magnetic fields, Astrophys. J., 188, 379, 1974.

Earl, J. A.: Analytical description of charged particle transport along arbitrary guiding field configurations, Astrophys. J., 252, 739, 1981.

Forman, M. A. and Webb, G. M.: Acceleration of energetic particles, in: Collisionless shocks in the heliosphere: a tutorial review, (Eds) Stone, R. G. and Tsurutani, B. T., American Geophysical Union Press, Washington D. C., 1985.

Frandsen, A. M. A., Connor, B. V., Van Amersfoort, J., and Smith, E. J.: The ISEE-C vector helium magnetometer, IEEE Trans. Geosci. Electron., GE-16, 195, 1978.

Galvin, A. B., Ipavich, F. M., Gloeckler, G., Hovestadt, D., Bame, S. J., Klecker, B., Scholer, M., and Tsurutani, B. T.: Solar wind ion charge states preceding a driver plasma, J. Geophys. Res., 92, 12 069, 1987.

Gary, S. P., Madland, C. D., and Tsurutani, B. T.: Electromagnetic ion beam instabilities II, Phys. Fluids, 28, 3691, 1985.

Ho, C. M., Tsurutani, B. T., Goldstein, B. E., Phillips, J. L., and Balogh, A.: Tangential discontinuities at high heliographic latitude ($\sim -80°$), Geophys. Res. Lett., 22, 3409, 1995.

Hovestadt, D., Gloeckler, G., Fan, C. Y., et al.: The nuclear and ionic charge distribution particle experiments on the ISEE-1 and ISEE-C spacecraft, IEEE Trans. Geosci. Electron., GE-16, 166, 1978.

Jokipii, J. R. and Coleman, Jr., P. J.: Cosmic ray diffusion tensor and its variation observed with Mariner 4, J. Geophys. Res., 73, 5495, 1968.

Kahler, S., Reames, D. V., Sheeley, Jr., N. R., Howard, R. A., Koomes, M. J., and Michaels, D. J.: A comparison of solar ^{3}Helium-rich evetns with Type II burst and coronal mass ejections, Astrophys. J., 290, 742, 1985.

Kennel, C. F. and Petschek, H. E.: Limit on stably trapped particle fluxes, J. Geophys. Res., 71, 1, 1966.

Klein, L. W. and Burlaga, L. F.: Interplanetary magnetic clouds at 1 AU, J. Geophys. Res., 87, 613, 1982.

Kuramitsu, Y. and Hada, T.: Acceleration of charged particles by large amplitude MHD waves: effect of wave spatial correlation, Geophys. Res. Lett., in press, 2000.

Landau, L. D. and Lifschitz, E. M.: Electrodynamics of continuous media, Addison Wesley, Massachusetts, 224, 1960.

Lyons, L. R., Thorne, R. M., and Kennel, C. F.: Pitch-angle diffusion of radiation belt electrons within the plasmasphere, J. Geophys. Res., 77, 3455, 1972.

Ma Sung, L. S. and Earl, J. A.: Interplanetary propagation of flare-associated energetic particles, Astrophys. J., 222, 1080, 1978.

Mason, G. M., Fisk, L. A., Gloeckler, G., and Hovestadt, D.: A survey of $\sim$1 MeV nucleon-1 solar flare particle abundances, $1 < Z, < 26$, during the 1973–1977 solar minimum period, Astrophys. J., 239, 1070, 1980.

Mason, G. M., Ng, C. K., Klecker, B., and Green, G.: Impulsive accelration and scatter-free transport of $\sim$1 MeV per nucleon ions in ^{3}He rich solar particle events, Astrophys. J., 339, 529, 1989.

Mason, G. M., Mazur, J. E., and Dwyer, J. R.: ^{3}He enhancements in large solar energetic particle events, Astrophys. J. Lett., 525, L133, 1999.

Mazur, J. E., Mason, G. M., Klecker, B., and McGuire, R. E.: The energy spectra of solar flare hydrogen, helium, oxygen and iron: evidence for stochastic acceleration, Astrophys. J., 40, 398, 1992.

Mazur, J. E., Mason, G. M., Klecker, B., and McGuire, R. E.: The abundances of hydrogen, helium, oxygen, and iron accelerated in large solar particle events, Astrophys. J., 404, 810, 1993.

Mazur, J. E., Mason, G. M., and Von Rosenvinge, T. T.: Fe-rich solar energetic particle events during solar minimum, Geophys. Res. Lett., 23, 1219, 1996.

Mazur, J. E., Mason, G. M., Dwyer, J. R., and Von Rosenvinge, T. T.: Solar energetic particles inside magnetic clouds observed with the Wind spacecraft, Geophys. Res. Lett., 25, 2521, 1998.

McDonald, F. B., Teegarden, B. J., J.H. Trainor, Von Rosenvinge, T. T., and Webber, W. R.: The interplanetary accleration of energetic nucleons, Astrophys. J., 203, L149, 1976.

McGuire, R. E., Von Rosenvinge, T. T., and McDonald, F. B.: The composition of solar energetic particles, Astrophys. J., 301, 938, 1986.

Ng, C. K. and Wong, K.-Y.: Solar particle propagation under the influence of pitch-angle diffusion and collation in the interplanetary magnetic field, in: Proc. 16th International Cosmic Ray Conference, Kyoto, Japan, 5, 252, 1979.

Ng, C. K. and Reames, D. V.: Focused interplanetary transport of $\sim$1 MeV solar energetic protons through self-generated Alfvén waves, Astrophys. J., 424, 1032, 1994.

Neugebauer, M., Clay, D. R., Goldstein, B. E., Tsurutani, B. T., and Zwickl, R. D.: A reexamination of ratational and tangential discontinuities in the solar wind, J. Geophys. Res., 89, 5395, 1984.

Neugebauer, M. C., Alexander, J., Schwenn, R., and Richter, A. K.: Tangential discontinuities in the solar wind: correlated field and velocity changes and the Kelvin-Helmholtz instability, J. Geophys. Res., 91, 13 694, 1986.

Palmer, I. D.: Transport coefficients of low-energy cosmic rays in interplanetary space, Rev. Geophys. Space Phys., 20, 335, 1982.

Pesses, M. E., Decker, R. B., and Armstrong, T. P.: The acceleration of charged particles in interplanetary shock waves, Space Sci. Rev., 32, 185, 1982.

Phillips, J. L., Bame, S. J., Feldman, W. C., et al.: Ulysses solar wind plasma observations at high southerly latitudes, Science, 268, 1030, 1995.

Ragot, B. T.: Nongyroresonant pitch angle scattering, Astrophys. J., 518, 974, 1999.

Ragot, B. T.: Parallel mean free path of solar cosmic rays, Astrophys. J., 536, 455, 2000.

Reames, D. V., Von Rosenvinge, T. T., and Lin, R. P.: Solar ^{3}He-rich events and nonrelativistic electron events: a new association, Astrophys. J., 272, 716, 1985.

Reames, D. V.: Waves generated in the transport of particles from large solar flares, Astrophys. J., L51, 342, 1989.

Reames, D. V.: Acceleration of energetic particles by shock waves from large solar flares, Astrophys. J., 358, L63, 1990a.

Reames, D. V.: Energetic particles from impulsive solar flares, Astrophys. J., 73, 235, 1990b.

Reames, D. V. and Ng, C. K.: Streaming-limited intensities of solar energetic particles, Astrophys. J., 504, 1002, 1998.

Roberts, D. A. and Goldstein, M.: Turbulence and waves in the solar wind, U.S. Nat. Rep. Int. Union Geol. Geophys., 1987–1990, Rev. Geophys. Suppl., 29, 932, 1991.

Roelof, E. C.: Propagation of solar cosmic rays in the interplanetary magnetic field, in: Lectures in High Energy Astrophysics, (Eds) Ogelmann, H. and Wayland, J. R., NASA SP-199, 111, 1969.

Schlickeiser, R.: Cosmic ray transport and acceleration, I. Derivation of the kinetic equation and application to cosmic ray in a static cold media, Astrophys. J., 336, 243, 1989.

Schlickeiser, R. and Miller, J. A.: Quasi-linear theory of cosmic ray transport and acceleration: the role of oblique magnetohydrodynamic waves and transit-time damping, Astrophys. J., 492, 352, 1998.

Sentman, D., Edmiston, J. P., and Frank, L. A.: Instabilities of low frequency, parallel propagating electromagnetic waves in the Earth's foreshock region, J. Geophys. Res., 86, 7487, 1981.

Siscoe, G. L., Davis, Jr., L., Coleman, Jr., P. J., Smith, E. J., and Jones, D. E.: Power spectra and discontinuities of the interplanetary magnetic field; Mariner 4, J. Geophys. Res., 73, 61, 1968.

Sanahuja, B., Lario, D., and Heras, A. M.: 24th Int. Cosmic Ray Conf., SH4, 1995.

Smith, E. J.: Identification of interplanetary tangential and ratational discontinuities, J. Geophys. Res., 78, 2054, 1973.

Smith, E. J. and Tsurutani, B. T.: Magnetosheath lion roars, J. Geophys. Res., 81, 2261, 1976.

Smith, E. J., Balogh, A., Neugebauer, M., and McComas, D.: Ulysses observations of Alfvén waves in the southern and northern hemispheres, Geophys. Res. Lett., 22, 3381, 1995.

Sonnerup, B. U. O. and Cahill, L. J.: Mantopause structure and attitude from Explorer 12 observatories, J. Geophys. Res., 72, 171, 1967.

Tan, L. C. and Mason G. M.: Magnetic field power spectra during "scatter-free" solar particle events, Astrophys. J. Lett., L29, 409,

1993.
Thomas, B. T. and Smith, E. J.: The Parker spiral configuration of the interplanetary magnetic field between 1 and 8.5 AU, J. Geophys. Res., 85, 6861, 1980.
Tsurutani, B. T., Smith, E. J., Pyle, K. R., and Simpson, J. A.: Energetic protons accelerated at corotating shocks: Pioneer 10 and 11 observations from 1 to 6 AU, J. Geophys. Res., 87, 7389, 1982.
Tsurutani, B. T. and Thorne, R. M.: Diffusion processes in the magnetosphere boundary layer, Geophys. Res. Lett., 9, 1247, 1982.
Tsurutani, B. T., Smith, E. J., and Jones, D. E.: Waves observed upstream of interplanetary shocks, J. Geophys. Res., 88, 5645, 1983.
Tsurutani, B. T., Gonzalez, W. D., Tang, F., Akasofu, S.-I., and Smith, E. J.: Origin of interplanetary southward magnetic fields responsible for major magnetic storms near solar maximum (1978–1979), J. Geophys. Res., 93, 8519, 1988.
Tsurutani, B. T.: Comets: a laboratory for plasma waves and instabilities, in: Cometary Plasma Processes, (Ed) Johnstone, A., American Geophysical Union Press, Washington D. C., 1991.
Tsurutani, B. T., Ho, C. M., Smith, E. J., Neugebauer, M., Goldstein, B. E., Mok, J. S., Arballo, J. K., Balogh, A., Southwood, D. J., and Feldman, W. C.: The relationship between interplanetary discontinuities and Alfvén waves: Ulysses observations, Geophys. Res. Lett., 21, 2267, 1994.
Tsurutani, B. T., Gonzalez, W. D., Gonzalez, A. L. C., Tang, F., Arballo, J. K., and Okada, M.: Interplanetary origin of geomagnetic activity in the declining phase of the solar cycle, J. Geophys. Res., 100, 21 717, 1995.
Tsurutani, B. T., Ho, C. M., Arballo, J. K., Smith, E. J., Goldstein, B. E., Neugebauer, M., Balogh, A., and Feldman, W. C.: Interplanetary discontinuities and Alfvén waves at high heliographic latitudes: Ulysses, J. Geophys. Res., 101, 11 027, 1996.
Tsurutani, B. T. and Gonzalez, W. D.: The future of geomagnetic storm predictions: implications from recent solar and interplanetary observations, J. Atmos. Terr. Phys., 57, 1369, 1995.
Tsurutani, B. T. and Lakhina, G. S.: Some basic concepts of wave-particle interactions in collisionless plasmas, Rev. Geophys., 35, 491, 1997.
Tsurutani, B. T., Arballo, J. K., Lakhina, G. S., Ho, C. M., Ajello, J., Pickett, J. S., Gurnett, D. A., Lepping, R. P., Peterson, W. K., Rostoker, G., Kamide, Y., and Kokubun, S.: The January 1997 coronal hot spot, horseshoe aurora and first substorm: a CME loop?, Geophys. Res. Lett., 25, 3047, 1998.
Tsurutani, B. T. and Ho, C. M.: A review of discontinuities and Alfvén waves in interplanetary space: Ulysses results, Rev. Geophys., 37, 514, 1999.
Tsurutani, B. T., Lakhina, G. S., Winterhalter, D., Arballo, J. K., Galvan, C., and Sakurai, R.: Energetic particle cross-field diffusion: interaction with magnetic decreases (MDs), Nonlin. Proc. Geophys., 6, 235, 2000.
Tsurutani, B. T., Buti, B., Galvan, C., Arballo, J. K., Winterhalter, D., Sakurai, R., Lakhina, G. S., Smith, E. J., and Balogh, A.: Relationship between discontinuities, magnetic holes, magnetic decreases, and nonlinear Alfvén waves: Ulysses observations over the solar poles, Geophys. Res. Lett., in press, 2001.
Tu, C.-Y. and Marsch, E.: A model of solar wind fluctuations with two components: Alfvén waves and convected structures, J. Geophys. Res., 78, 1257, 1993.
Valdes-Galicia, J. F. and Alexander, P.: Is it possible to find evidence of waves generated by solar energetic protons?, Sol. Phys., 176, 327, 1997.
Wanner, W. and Wibberenz, G.: A study of the propagation of solar energetic particles in the inner heliosphere, J. Geophys. Res., 98, 3513, 1993.
Wanner, W., Kallenrode, M. B., Droge, W., and Wibberenz, G.: Solar energetic proton mean free paths, Adv. Space Res., 13, 359, 1993.
Wanner, W., Jaekel, J., Kallenrode, M.-B., Wibberenz, G., and Schlikeiser, R.: Observational evidence for a spurious dependence of slab QLT proton mean free paths on the magnetic field angle, Astron. Astrophys., 290, L5, 1994.
Yoon, P. C., Ziebell, L. F., and Wu, C. S.: Self-consistent pitch angle diffusion of new born ions, J. Geophys. Res., 96, 5469, 1991.
Zhang, G. and Burlaga, L. F.: Magnetic clouds, geomagnetic disturbances, and cosmic ray decreases, J. Geophys. Res., 93, 2511, 1988.
Zwickl, R. D. and Webber, W. R.: Solar particle propagation from 1 to 5 AU, Sol. Phys., 54, 457, 1977.
Zwickl, R. D., Roelof, E. C., Gold, R. E., and Krimigis, S. M.: Z-rich solar particle event characteristics 1972–1976, Astrophys. J., 225, 281, 1978.
Zwickl, R. D., Asbridge, J. R., Bame, S. J., Feldman, W. C., Gosling, J. T., and Smith, E. J.: Plasma properties of driver gas following interplanetary shocks observed by ISEE-3, Solar Wind Five, NASA Conf. Publ., CP-2280, 711, 1983.